Does stress transmission in forelands depend on structural style? Distinctive stress magnitudes during Sevier thin-skinned and Laramide thick-skinned layer-parallel shortening in the Bighorn Basin (USA) revealed by stylolite and calcite twinning paleopiezometry

Nicolas Beaudoin, Olivier Lacombe, Marie-Eléonore David, Daniel Koehn

Does stress transmission in forelands depend on structural style ? Distinctive stress magnitudes during Sevier thin-skinned and Laramide thick-skinned layer-parallel shortening in the Bighorn Basin (USA) revealed by stylolite and calcite twinning paleopiezometry.

Nicolas Beaudoin[1], Olivier Lacombe[2], Marie-Eléonore David[2], Daniel Koehn[3].

[1] *Université de Pau et des Pays de l'Adour, E2S UPPA, CNRS, TOTAL, LFCR, Pau, France*

[2] *Sorbonne Université, CNRS-INSU, Institut des Sciences de la Terre de Paris, ISTeP UMR 7193, F-75005 Paris, France*

[3] *GeoZentrum Nordbayern, University Erlangen-Nuremberg, Schlossgarten 5, 91054, Erlangen, Germany*

ABSTRACT

The Sheep Mountain – Little Sheep Mountain Anticlines, Bighorn Basin (USA) formed as basement-cored Laramide structures in the formerly undeformed foreland of the thin-skinned Sevier orogen. We take advantage of the well constrained microstructural network there to reconstruct differential stress magnitudes that prevailed during both Sevier and Laramide Layer-Parallel Shortening (LPS), before the onset of large-scale folding. Differential stress magnitudes determined from tectonic stylolites are compared and combined to previous stress estimates from calcite twinning paleopiezometry in the same formations. During stress loading related to LPS, differential stress magnitudes transmitted from the distant Sevier thin-skinned orogen into the sedimentary cover of the Bighorn basin (11-43 MPa) are higher than the differential stress magnitudes accompanying the early stage of LPS related to the thick-skinned

Laramide deformation (2-19 MPa). This study illustrates that the tectonic style of an orogen affects the transmission of early orogenicstress into the stable continental interior.

INTRODUCTION

Providing quantitative estimates of the evolution of past stress magnitudes over time is a challenging task, albeit important to understand the long-term mechanical and paleohydrological behaviour of the upper crust. While strain mostly distribute at plate boundaries, there is a significant intraplate stress transmission thousands of kilometers away from the source of the stress that leads to the development of mesostructures such as fractures or stylolites before and/or beyond macrostructures such as folds and thrusts (Lacombe and Mouthereau, 1999; Tavani et al., 2015; Weil and Yonkee, 2012). The use of calcite twinning paleopiezometry documented an overall cratonward decrease in orogenic stress, with a drop of differential stress ($\sigma_d = \sigma_1-\sigma_3$) values in the first hundred kilometers from the orogen hinterland/foreland boundary (>100 MPa to 20 MPa; Beaudoin and Lacombe, 2018). The reason of this stress transmission pattern, and its dependence on the orogenic tectonic style are still debated (Van der Pluijm et al., 1997; Lacombe, 2010). In order to tackle this issue, we combined existing stress data from calcite twinning paleopiezometry (Amrouch et al., 2010) with original σ_d values obtained from stylolite roughness paleopiezometry (Ebner et al., 2010b; Schmittbuhl et al., 2004) from the sedimentary cover of the Sheep Mountain-Little Sheep Mountain anticlines (Bighorn Basin, Wyoming, USA; Fig. 1) where the network of systematic veins/mesoscale faults and paleostress reconstructions document two stages of layer-parallel shortening (LPS), related to thin-skinned (i.e., basement remaining undeformed) then to thick-skinned (i.e., involving the basement) tectonics.

GEOLOGICAL SETTING

The Bighorn Basin belongs to the thick-skinned Laramide Province of the Rocky Mountains (Fig. 1C) that formed by latest Cretaceous until Paleogene times in response to the flat-slab subduction of the Farallon plate (Yonkee and Weil, 2015). Micro/meso-structural studies combined with absolute dating of vein cements (Amrouch et al., 2010; Beaudoin et al., 2012; Beaudoin et al., 2014; Beaudoin et al., 2018; Bellahsen et al., 2006a; Craddock and van der Pluijm, 1999; Neely and Erslev, 2009; Varga, 1993; Weil and Yonkee, 2012; Yonkee and Weil, 2010) show that the sedimentary strata of the Bighorn Basin recorded (1) pre-Laramide LPS, related to compressive stress likely transmitted from the distant thin-skinned Sevier orogen at the time the basin was still part of the Sevier undeformed foreland (vein set S, $\sigma 1$ striking WNW-ESE prior to folding, 81-72 Ma, Fig. 2A); (2) Laramide LPS (vein set L-1, $\sigma 1$ striking NE-SW prior to folding, 72-50 Ma, Fig. 2A); (3) Laramide thrust-related, basement-cored folding with veins developed at fold hinges (vein Set L-2, 50-35 Ma, Fig. 2A). Field observations also document the occurrence of bed perpendicular tectonic stylolites with peaks oriented (1) ~WNW-ESE and (2) NE-SW after unfolding (Fig. 2B, 2C, Amrouch et al., 2010; 2011). The orientations of the stylolite peaks, commonly considered as reliable markers of the orientation of the tectonic stress (eg, Koehn et al., 2007; Tavani et al., 2015; Weil and Yonkee, 2012), together with their kinematic compatibility and chronological relationships with the veins of set S and L-1, respectively (Fig. 2C), and with the conjugate reverse and strike-slip mesoscale faults that also developed during Laramide LPS (Amrouch et al., 2011; Amrouch et al., 2010) unambiguously support that these tectonic stylolites witness the successive horizontal compressive stress related to the Sevier and Laramide events, respectively.

STYLOLITE ROUGHNESS INVERSION FOR STRESS

Stylolites are serrated surfaces (Fig. 2B) that develop by chemical dissolution under stress (Alvarez et al., 1978; Fletcher and Pollard, 1981; Koehn et al., 2007; Toussaint et al.,

2018). The growth and the morphology of a stylolite are rate-dependent (e.g., Stockdale, 1922); they are governed by the kinetics of dissolution and the distribution of heterogeneities, and are affected by the amount of clay enhancing the dissolution (Renard et al., 2001). Once dissolution starts, there is a thermodynamic competition between (1) a destabilizing (roughening) force due to pinning particles on the stylolite surface that resist dissolution, and (2) stabilizing (smoothening) forces, long-range elastic forces and local surface tension that tend to flatten the stylolite surface by preferentially dissolving areas of local roughness (Schmittbuhl et al., 2004). While the topography of the stylolite during its growth is sensitive to both strain rate and stress (Koehn et al., 2012), the final topography of a stylolite is a saturation state that is reached over a short period of time, ca. 200 years (Schmittbuhl et al., 2004) at the end of dissolution due to local drop in solubility (Rolland et al., 2012). Hence the final roughness, *i.e.* the difference in height between two points along the stylolite plane, reflects the ambient stress at the time pressure-dissolution stopped, and is dependent on neither strain rate nor lithology (Ebner et al., 2009).

The stress inversion technique relies upon a fractal analysis of high-resolution 2D scans (12800 dpi) of the final roughness on the stylolite surface. In most cases, the 1D topography of a stylolite is best described by a self-affine scaling invariance (Schmittbuhl et al., 2004), i.e. the rough shape is invariant under a range of scales. A classic way to determine the self-affinity of a signal is to analyze it with a Fourier power spectrum, that relates the wave number k (mm^{-1}) to the squared Fourier transform modulus P(k) as $P(k) \propto k^{2H+1}$, where H is the roughness (or Hurst) exponent (Barabási and Stanley, 1995). In the case of stylolites, such analysis typically exhibits 2 power laws (Fig. 3A): a large-scale (usually > 1mm) law with a specific roughness exponent of 1.1 which reflects the elastic energy dominated regime; and a small-scale law with a specific roughness exponent of 0.5 which reflects the surface energy dominated regime. A third part of the data forms a flat tail at the lowest scales that reflects a resolution effect related

to image treatment (Fig. 3A). The scale of observation at which the self-affine invariance switches from one power law to the other one, defined as the crossover length L_c, is directly linked to the absolute magnitude of the mean and differential stresses (σ_m and σ_d, respectively) that prevailed at the end of the life of a stylolite as $L_c = \frac{\gamma E}{\beta \sigma_m \sigma_d}$, with E the Young's modulus (Pa), γ the solid-fluid interfacial energy (J.m^{-2}), and β a dimensionless constant β= ν(1-2ν)/π with ν being the Poisson's ratio (Schmittbuhl et al., 2004).

The evolution of the topography and related L_c on tectonic stylolite surfaces exhibits a periodic anisotropy of the L_c (Ebner et al., 2010b) that can be reconstructed from a minimum of three cuts normal to the surface if one knows the mechanical/chemical parameters of the dissolved rock (Fig. 3B; Beaudoin et al., 2016). If the reconstructed anisotropy returns minima and maxima aligned with the vertical and horizontal directions (Fig. 3D), then it provides access to the horizontal crossover length L_h and to the vertical crossover length L_v, which yield the magnitudes of the horizontal maximum (σ_H) and minimum (σ_h) stresses as $\frac{L_h}{L_v} = \frac{\sigma_H - \sigma_v}{\sigma_H - \sigma_h}$, provided the vertical stress σ_v (i.e., the weight of overburden) is known (Ebner et al., 2010b).

SAMPLING STRATEGY AND RESULTS

Because stylolite occurrence depends on lithology (Marshak and Engelder, 1985) and to limit the variability of rock type and mechanical properties of samples, Sevier and Laramide-related tectonic stylolites were collected at different structural locations solely in the partly dolomitized, grainstone facies of the Mississippian Madison Formation and of the Permian Phosphoria Formation (Barbier et al., 2012; Fig. 1A).

Three peak-parallel cuts were done for each stylolite with an angle between each cut (Table 1), and each roughness signal was inverted using the Fourier power spectrum (Fig.3C)(Ebner et al., 2010a; Renard, 2004). The L_c anisotropy was reconstructed from the three values of L_c (Fig.3D) (Beaudoin et al., 2016). Successful inversion comprises 13 tectonic

stylolites (Table 1, Figs. S1, S2, S3) sampled in the Madison Formation (n=10) and in the Phosphoria Formation (n=3).

To determine σ_d values, we considered a range of depths of deformation obtained by comparing published basin models (Beaudoin et al., 2014b; May et al., 2013) with the range of absolute U-Pb ages of the systematic veins S and L-1 related to Sevier and Laramide LPS (Beaudoin et al., 2018). This reveals that the Madison Formation was buried at depths of 1500-2450 m and 2450-2800m at the time of Sevier and Laramide LPS, respectively (and we consider an average of 300 m less for the Phosphoria Fm.). We also use Poisson ratio and Young modulus obtained from mechanical tests on the Phosphoria and Madison Formations from Sheep Mountain (Amrouch et al., 2011, Table 1) and the classic solid-fluid interfacial energy value for dolomite (0.24 $J.m^{-2}$, Wright et al., 2001). The L_c is estimated assuming a linear-by-parts fit of the Fourier spectra modelled by a least square algorithm (Ebner et al., 2009). Such analytical solution returns the L_c within a 23% uncertainty (Rolland et al., 2014), that can be considered as the maximum methodological uncertainty as other parameters are known. Note that an extra source of uncertainties can be found in the modelling of the periodic anisotropy from 3 cuts (Beaudoin et al., 2016).

Laramide-related σ_d values (n=8) range from 2±0.5 MPa to 19±4.4 MPa (n=7) while Sevier-related σ_d values (n=5) range from 11±2.2 MPa to 24±4.8 MPa (n=6).

DISCUSSION AND CONCLUSIONS

σ_d estimates from inversion of the roughness of tectonic stylolites were compared with published σ_d estimates from calcite twinning paleopiezometry in the same formations (Fig. 4) (Amrouch et al., 2010). We discarded the published σ_d values from calcite twinning paleopiezometry interpreted as reflecting local stress perturbations at the tip of the upward

propagating Laramide thrust (Amrouch et al., 2010; Bellahsen et al., 2006b) rather than the regional stress field of interest.

To account for the fact σd values inferred from tectonic stylolites are systematically lower than those inferred from calcite twinning when considering each deformation event (i.e. Sevier or Laramide)(Fig.4), we propose that stylolite development mostly predates vein formation and calcite twinning strain in a stress build-up model. This sequence could be the reason why the local stress perturbation above the tip of the basement fault is not recorded by the tectonic stylolites.We propose that during stress build-up in the flat-lying strata, pressure-solution initiated with low σ_d along planar solubility heterogeneities in rocks (such as elongated pores) and halted rapidly, presumably by clogging around the dissolution planes (Toussaint et al., 2018). Stylolites would have therefore dissipated the earliest part of the stress build-up before saturating. Then, because increasing stress would not have been accommodated fully by pressure-solution, stress would have accumulated enough to trigger vein development and calcite twinning, until newly-formed mesoscale faulting ultimately took place if the required σ_d was reached.

Integration of both paleopiezometers highlights that most σ_d values related to Sevier LPS (11±2.2 to 43±9 MPa) are notably higher than σ_d values (2±0.5 to 19±4 MPa) related to Laramide LPS. The results document for the first time a systematic difference in σ_d magnitudes sustained by flat-lying strata at the same place in relation to the evolving deformation style over time. The σ_d values derived from both paleopiezometers reflect the σ_d prevailing at the burial depth at which the strata underwent LPS. Because the depth of deformation of strata was larger during the Laramide LPS than during the Sevier LPS (Δ_{depth}~ 650m on average, Table 1) and since σ_d increases with depth (Lacombe, 2007; Beaudoin and Lacombe, 2018), the normalization to a similar depth simply increases the difference between σ_d values associated

with the Sevier and the Laramide LPS, thus confirming that this difference in σ_d values reflects a significant trend.

We propose that the stress recorded in the Bighorn Basin was first efficiently transmitted from the distant Sevier thin-skinned orogen into the stable foreland through a shallow stress guide, i.e., the sedimentary cover (Fig. 4), reaching values compatible with the σ_d values derived from calcite twins for the Sevier foreland elsewhere (20-40 MPa, van der Pluijm et al., 1997). We further propose that the low Laramide σ_d reconstructed in the cover rocks represents only a fraction of the source stress transmitted forelandward through a deep (crustal or lithospheric) stress guide (Fig. 4) (Erslev, 1993). We speculate that most of the stress was dissipated at depth while triggering the inversion of inherited basement normal faults (Lacombe and Bellahsen, 2016; Marshak et al., 2000). and so as it was transmitted upward into the attached cover during the early stage of Laramide LPS, ~20 Ma after the onset of exhumation of Laramide basement arches (Beaudoin et al., 2019), the Laramide LPS-related σ_d remained much lower compared to former Sevier σ_d values. It was only at the time of later generalized Laramide large-scale basement-cored folding that σ_d strongly increased to reach their maximum values in the cover rocks (Amrouch et al., 2011).

This study therefore illustrates that the tectonic style of an orogen affects the magnitude of the σ_d transmitted toward the stable continental interior and therefore challenges previous models of cratonward decrease of σ_d regardless of the structural style of the orogen. Beyond regional implications, this study further establishes tectonic stylolite roughness inversion as a reliable and powerful paleopiezometer to constrain stress build-up in poorly deformed strata of stable orogenic forelands, which places it as a useful complement of calcite twinning paleopiezometry.

ACKNOWLEDGMENTS

This work was funded by Sorbonne Université (research agreement C14313) and by the European Union Seventh Framework Programme for research, technological development and demonstration (grant agreement n°316889). NB is funded through the ISITE program E2S, supported by ANR PIA and Région Nouvelle-Aquitaine. Authors thank Stephen Marshak, Adolf Yonkee, Atilla Aydin and two anonymous reviewers for their constructive comments that greatly improved the manuscript, as well as the science editor Jean Braun.

REFERENCES

Alvarez, W., Engelder, T., and Geiser, P. A., 1978. Classification of solution cleavage in pelagic limestones: Geology, v. 6, no. 5, p. 263-266.

Amrouch, K., Beaudoin, N., Lacombe, O., Bellahsen, N., and Daniel, J.-M., 2011. Paleostress magnitudes in folded sedimentary rocks: Geophysical Research Letters, v. 38, no. 17, L17301.

Amrouch, K., Lacombe, O., Bellahsen, N., Daniel, J.-M., and Callot, J.-P., 2010. Stress and strain patterns, kinematics and deformation mechanisms in a basement-cored anticline: Sheep Mountain Anticline, Wyoming: Tectonics, v. 29, no. 1, TC1005.

Barabási, A. and Stanley, H. 1995. *In:* Fractal Concepts in Surface Growth, Barabási, A. and Stanley, H. (eds), Cambridge University Press, Cambridge, 366 pp.

Barbier, M., Hamon, Y., Callot, J.-P., Floquet, M., Daniel, J.-M., 2012. Sedimentary and diagenetic controls on the multiscale fracturing pattern of a carbonate reservoir: The Madison Formation (Sheep Mountain, Wyoming, USA). Marine and Petroleum Geology 29, 50-67.

Beaudoin, N., Bellahsen, N., Lacombe, O., Emmanuel, L., and Pironon, J., 2014a. Crustal-scale fluid flow during the tectonic evolution of the Bighorn Basin (Wyoming, USA): Basin Research, v. 26, no. 3, p. 403-435.

Beaudoin, N., Koehn, D., Lacombe, O., Lecouty, A., Billi, A., Aharonov, E., and Parlangeau, C., 2016. Fingerprinting stress: Stylolite and calcite twinning paleopiezometry revealing the complexity of progressive stress patterns during folding-The case of the Monte Nero anticline in the Apennines, Italy: Tectonics, v. 35, no. 7, p. 1687-1712.

Beaudoin, N., and Lacombe, O., 2018. Recent and future trends in paleopiezometry in the diagenetic domain: Insights into the tectonic paleostress and burial depth history of fold-and-thrust belts and sedimentary basins: Journal of Structural Geology, v. 114, p. 357-365.

Beaudoin, N., Lacombe, O., Bellahsen, N., Amrouch, K., and Daniel, J.-M., 2014b. Evolution of pore-fluid pressure during folding and basin contraction in overpressured reservoirs: Insights from the Madison–Phosphoria carbonate formations in the Bighorn Basin (Wyoming, USA): Marine and Petroleum Geology, v. 55, p. 214-229.

Beaudoin, N., Lacombe, O., Roberts, N. M. W., and Koehn, D., 2018. U-Pb dating of calcite veins reveals complex stress evolution and thrust sequence in the Bighorn Basin, Wyoming, USA: Geology, v. 46, no. 11, p. 1015-1018.

Beaudoin, N., Lacombe, O., Roberts, N. M. W., and Koehn, D., 2019. U-Pb dating of calcite veins reveals complex stress evolution and thrust sequence in the Bighorn Basin, Wyoming, USA: REPLY: Geology, e481, https://doi.org/10.1130/G46606Y.1.

Beaudoin, N., Leprêtre, R., Bellahsen, N., Lacombe, O., Amrouch, K., Callot, J.-P., Emmanuel, L., and Daniel, J.-M., 2012. Structural and microstructural evolution of the Rattlesnake Mountain Anticline (Wyoming, USA): New insights into the Sevier and Laramide orogenic stress build-up in the Bighorn Basin: Tectonophysics, v. 576-577, p. 20-45.

Bellahsen, N., Fiore, P., and Pollard, D. D., 2006a. The role of fractures in the structural interpretation of Sheep Mountain Anticline, Wyoming: Journal of Structural Geology, v. 28, no. 5, p. 850-867.

Bellahsen, N., Fiore, P. E., and Pollard, D. D., 2006b. From spatial variation of fracture patterns to fold kinematics: A geomechanical approach: Geophysical Research Letters, v. 33, no. 2.

Craddock, J. P., and van der Pluijm, B. A., 1999. Sevier–Laramide deformation of the continental interior from calcite twinning analysis, west-central North America: Tectonophysics, v. 305, p. 275-286.

Ebner, M., Koehn, D., Toussaint, R., Renard, F., and Schmittbuhl, J., 2009. Stress sensitivity of stylolite morphology: Earth and Planetary Science Letters, v. 277, no. 3-4, p. 394-398.

Ebner, M., Piazolo, S., Renard, F., and Koehn, D., 2010a. Stylolite interfaces and surrounding matrix material: Nature and role of heterogeneities in roughness and microstructural development: Journal of Structural Geology, v. 32, no. 8, p. 1070-1084.

Ebner, M., Toussaint, R., Schmittbuhl, J., Koehn, D., and Bons, P., 2010b. Anisotropic scaling of tectonic stylolites: A fossilized signature of the stress field?: Journal of Geophysical Research, v. 115, no. B6, p. B06403.

Erslev, E. A., 1993. Thrusts, back-thrusts, and detachment of Rocky Mountain foreland arches: Geological Society of America Special Paper, v. 280, p. 339-358.

Fletcher, R. C., and Pollard, D. D., 1981. Anticrack model for pressure solution surfaces: Geology, v. 9, p. 419-424.

Koehn, D., Ebner, M., Renard, F., Toussaint, R., and Passchier, C. W., 2012. Modelling of stylolite geometries and stress scaling: Earth and Planetary Science Letters, v. 341-344, p. 104-113.

Koehn, D., Renard, F., Toussaint, R., and Passchier, C., 2007. Growth of stylolite teeth patterns depending on normal stress and finite compaction: Earth and Planetary Science Letters, v. 257, no. 3-4, p. 582-595.

Lacombe, O., 2007. Comparison of paleostress magnitudes from calcite twins with contemporary stress magnitudes and frictional sliding criteria in the continental crust: Mechanical implications: Journal of Structural Geology, v. 29, no. 1, p. 86-99.

Lacombe, O., 2010. Calcite Twins, a Tool for Tectonic Studies in Thrust Belts and Stable Orogenic Forelands: Oil & Gas Science and Technology – Revue d'IFP Energies nouvelles, v. 65, no. 6, p. 809-838.

Lacombe, O., and Bellahsen, N., 2016. Thick-skinned tectonics and basement-involved fold–thrust belts: insights from selected Cenozoic orogens: Geological Magazine, v. 153, no. 5-6, p. 763-810.

Lacombe, O. and Mouthereau, F., 1999. What is the real front of orogens ? The Pyrenean orogen as a case study. C. R. Acad. Sc., t. 329, II, 889-896

Marshak, S., and Engelder, T., 1985. Development of cleavage in limestones of a fold-thrust belt in eastern New York: Journal of Structural Geology, v. 7, no. 3-4, p. 345-359.

Marshak, S., Karlstrom, K., and Timmons, J. M., 2000. Inversion of Proterozoic extensional faults: An explanation for the pattern of Laramide and Ancestral Rockies intracratonic deformation, United States: Geology, v. 28, no. 8, p. 735-738.

May, S. R., Gray, G. G., Summa, L. L., Stewart, N. R., Gehrels, G. E., and Pecha, M. E., 2013. Detrital zircon geochronology from the Bighorn Basin, Wyoming, USA: Implications

for tectonostratigraphic evolution and paleogeography: Geological Society of America Bulletin, v. 125, no. 9-10, p. 1403-1422.
Neely, T. G., and Erslev, E. A., 2009. The interplay of fold mechanisms and basement weaknesses at the transition between Laramide basement-involved arches, north-central Wyoming, USA: Journal of Structural Geology, v. 31, no. 9, p. 1012-1027.
Renard, F., 2004. Three-dimensional roughness of stylolites in limestones: Journal of Geophysical Research, v. 109, no. B3, p. B03209.
Renard, F., Dysthe, D., Feder, J., Bjørlykke, K., and Jamtveit, B., 2001. Enhanced pressure solution creep rates induced by clay particles: Experimental evidence in salt aggregates: Geophysical Research Letters, v. 28, no. 7, p. 1295-1298.
Rolland, A., Toussaint, R., Baud, P., Conil, N., and Landrein, P., 2014. Morphological analysis of stylolites for paleostress estimation in limestones: International Journal of Rock Mechanics and Mining Sciences, v. 67, p. 212-225.
Rolland, A., Toussaint, R., Baud, P., Schmittbuhl, J., Conil, N., Koehn, D., Renard, F., and Gratier, J.-P., 2012. Modeling the growth of stylolites in sedimentary rocks: Journal of Geophysical Research: Solid Earth, v. 117, no. B6, p. B06403.
Schmittbuhl, J., Renard, F., Gratier, J. P., and Toussaint, R., 2004. Roughness of stylolites: implications of 3D high resolution topography measurements: Phys Rev Lett, v. 93, no. 23, p. 238501.
Stockdale, P. B., 1922. Stylolites: their nature and origin-PhD: Indiana University, 97 p.
Tavani,. S., Storti, S., Lacombe, O., Corradetti, A., Muñoz, J. A., and Mazzoli, S., 2015. A review of deformation pattern templates in foreland basin systems and fold-and-thrust belts: Implications for the state of stress in frontal regions of thrust wedges. Earth-Sciences Reviews, 141, 82-104.
Toussaint, R., Aharonov, E., Koehn, D., Gratier, J. P., Ebner, M., Baud, P., Rolland, A., and Renard, F., 2018. Stylolites: A review: Journal of Structural Geology, v. 114, p. 163-195.
van der Pluijm, B. A., Craddock, J. P., Graham, B. R., and Harris, J. H., 1997. Paleostress in Cratonic North America: Implications for Deformation of Continental Interiors: Science, v. 277, p. 794-796.
Varga, R. J., 1993. Rocky Mountain foreland uplifts: Products of a rotating stress field or strain partitioning?: Geology, v. 21, no. 12, p. 1115-1119.
Weil, A. B., and Yonkee, W. A., 2012. Layer-parallel shortening across the Sevier fold-thrust belt and Laramide foreland of Wyoming: spatial and temporal evolution of a complex geodynamic system: Earth and Planetary Science Letters, v. 357-358, p. 405-420.
Wright, K., Cygan, R.T., Slater, B., 2001. Structure of the (1014) surfaces of calcite, dolomite and magnesite under wet and dry conditions. Physical Chemistry Chemical Physics 3, 839-844.
Yonkee, W. A., and Weil, A. B., 2015. Tectonic evolution of the Sevier and Laramide belts within the North American Cordillera orogenic system: Earth-Science Reviews, v. 150, p. 531-593.
Yonkee, W. A. and Weil, A. B., 2010. Reconstructing the kinematic evolution of curved mountain belts: Internal strain patterns in the Wyoming salient, Sevier thrust belt, USA: Geological Society of America Bulletin, v. 122(1-2), p.24-49.

FIGURE:

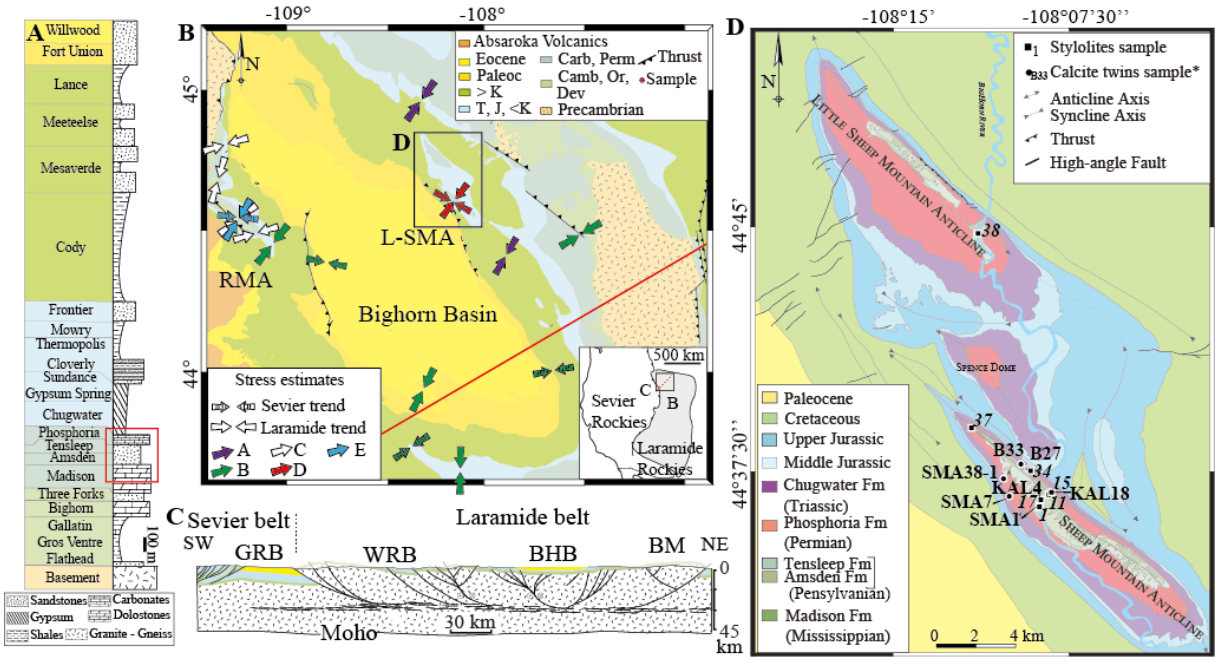

Figure 1: A- Stratigraphic column of the Bighorn Basin, modified after Neely and Erslev (2009). Red frames correspond to the studied formations, colors are related to the age of the formations following the key presented in B. B- Geological map of the Bighorn Basin (Wyoming, USA), the insert shows the location of the area with regard to simplified tectonic provinces, it also shows the location of the map B as a black frame and of the cross-section C as a red line. The reconstructed orientations of the horizontal maximum principal stress are reported as plain arrows for the Laramide event, and as crossed arrows for the Sevier event. Orientations are from: A: Varga (1993), B: Craddock and Van der Pluijm (1999), C: Neely and Erslev (2009), D: Amrouch et al. (2010), E: Beaudoin et al. (2012). C - cross section modified after Marshak et al. (2000). D- Simplified geological maps of the Little Sheep Mountain – Sheep Mountain anticline. Location of sampling sites for tectonic stylolite paleopiezometry and for calcite twinning paleopiezometry are reported as numbered squares and labelled circles, respectively (* from Amrouch et al., 2010).

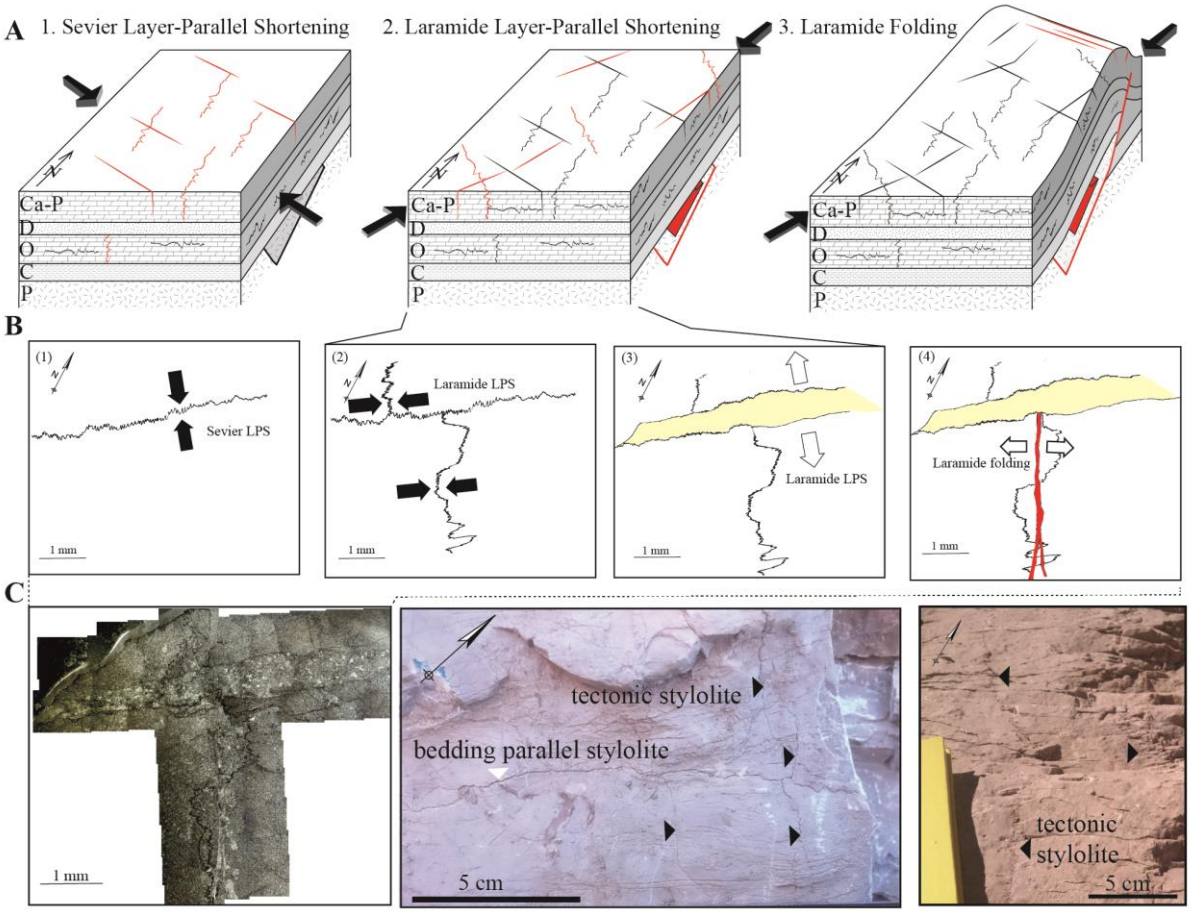

Figure 2: A- Schematic diagrams reporting the compressional trend, mode I veins (sets S, L-1, L-2), and stylolites developed during the Sevier LPS (1), the Laramide LPS (2), and the Laramide folding (3). The pre-existing structures are reported in black, the developing ones in red. For the sake of clarity, we omitted the Triassic-Paleogene overlying strata. P: Precambrian basement, C: Cambrian, O: Ordovician, D: Devonian, Ca-P: Carboniferous and Permian. B- sketch of microstructural observations proposing a possible sequence between tectonic stylolites with peaks oriented (1) WNW-ESE and (2) NE-SW and between veins oriented (3) NE-SW and (4) NW-SE, based on observed abutment and reopening relationships and supported by the general Sevier-Laramide sequence of deformation. C- On the right-hand side, microphotograph of the thin section on which sequence B was built. On the left-hand side, field photographs of tectonic and bedding parallel stylolites in the Madison Formation at Sheep Mountain Anticline.

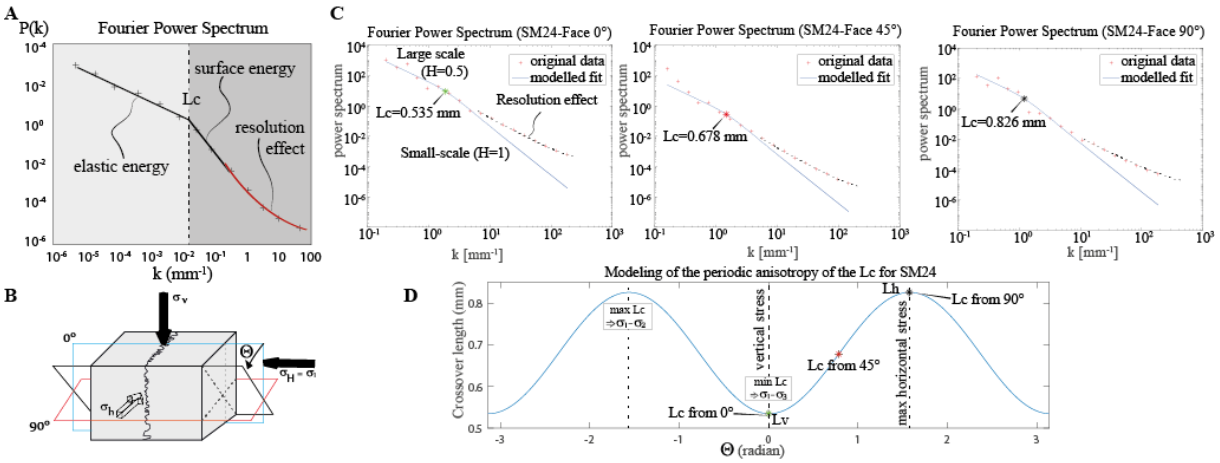

Figure 3: A – Ideal example of Fourier power spectrum applied to 1D profile of stylolite roughness, showing the different expected power laws and where the crossover length sits. B – Sketch of the cuttings through a tectonic stylolite in order to access the stylolite-plane anisotropy (after Beaudoin et al., 2016). C – Example of treatment for 3 cuts on the sample SM24, crossover lengths L_c are reported as coloured crosses within 23% uncertainty. D- Reconstructed periodic anisotropy of the Lc for the Sample SM24, using the L_c and angles presented in C. Similar dataset are presented for all samples as Figs. S1-S2-S3.

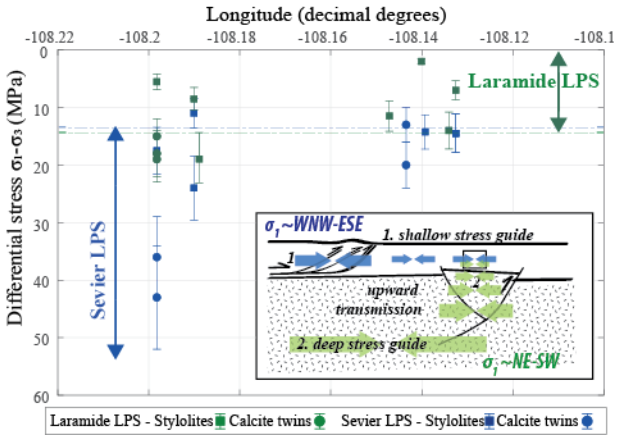

Figure 4: Location of samples (according to their longitude in decimal degrees) vs differential stress magnitudes (σ_1-σ_3, MPa) obtained from inversion of tectonic stylolite roughness (squares) and calcite twinning (circles). Green data points represent the Laramide-related σ_d, and the blue data points represent the Sevier-related σ_d. Error bars on squares account for the

overall uncertainty for each method. Double arrows and dashed lines represent the range of σ_d exclusive to Laramide layer-parallel shortening (green) and to Sevier layer-parallel shortening (blue), considering uncertainties. Insert is a conceptual model of stress transmission through shallow and deep stress guides that accounts for the difference in σ_d magnitudes sustained by sedimentary cover rocks during thin-skinned Sevier and thick-skinned Laramide LPS. Compressive stress related to Sevier (1) and Laramide (2) layer-parallel shortening is reported as blue and green convergent arrows, respectively, with larger size reflecting qualitatively higher σ_d. LPS – Layer Parallel Shortening

TABLE 1 Location of samples and results of inversion of tectonic stylolite roughness for stress in the Little Sheep Mountain – Sheep Mountain anticlines, USA.

Sample name and location						Teeth	Angle of cut (°)	Lc from FPS * (mm)	Anisotropy of Lc*		Depth ** (m)	Main principal stress magnitude (MPa)			Average Differential Stress (MPa)	Stress Ratio
Name	GPS	Longitude	Latitude	Formation	Bedding	Orientation[1]			Lv	Lh		σ_1	σ_2	σ_3		
Little Sheep Mountain Anticline																
LSM-S6	38	-108.19008	44.741	Madison	horizontal	N120	0	0.968	0.968	0.163	1500	nan	**35**	nan	24	0,17
							50	0.504			2450	62	**58**	38		
							90	0.163								
LSM-S13	38	-108.19008	44.741	Madison	horizontal	N105	0	0.643	0.28	0.57	1500	52	44	**35**	14	0,47
							90	0.471			2450	69	63	**58**		0,55
							140	0.287								
LSM-S11	38	-108.19008	44.741	Madison	horizontal	N042	0	0.394	0.36	0.64	2450	67	62	**58**	8,5	0,56
							15	0.368			2800	74	70	**66**		0,5
							90	0.619								
LSM-S16	38	-108.19008	44.741	Madison	horizontal	N045	0	0.231	0.15	0.74	2450	78	73	**58**	19	0,25
							90	0.666			2800	84	80	**66**		0,22
							75	0.535								
Sheep Mountain Anticline																
SM-S1	1	-108.13924	44.606	Madison	068-16S	N110	0	0.401	0.38	0.84	1500	48	42	**35**	11	0,46
							60	0.649			2450	67	63	**58**		0,44
							90	0.829								
SM-S22-1	15	-108.13253	44.615	Madison	120-64N	N113	0	0.725	0.27	1,56	1500	52	49	**35**	14,5	0,18
							45	0.294			2450	70	67	**58**		0,25
							90	1.025								
SM-S22-2	15	-108.13253	44.615	Madison	120-64N	N130	0	0.424	0.42	0.59	1500	52	49	**35**	14,5	0,18
							90	0.59			2450	70	67	**58**		0,25
							125	0.537								
SM-S31	37	-108.19825	44.649	Phosphoria	125-36W	N140	0	0.397	0.37	0.78	1250	50	40	**29**	17,5	0,48
							60	0.591			2250	67	60	**53**		0,5
							90	0.726								
SM-S18	11	-108.13253	44.615	Madison	145-47E	N040	0	0.3	0.22	0.52	2450	73	66	**58**	14	0,47
							90	0.493			2800	79	74	**66**		0,38
							120	0.515								
SM-S10	17	-108.14007	44.611	Madison	113-17S	N045	0	1.996	1.62	4.36	2450	60	59	**58**	2	0,5
							45	2.451			2800	68	67	**66**		0,5
							90	4								
SM-S24	34	-108.14711	44.622	Phosphoria	120-76S	N045	0	0.535	0.535	0.826	2300	66	57	**54**	11,5	0,75
							45	0.678			2600	72	65	**61**		0,64
							90	0.826								
SM-S32	37	-108.19825	44.649	Phosphoria	125-36W	N045	0	0.902	0.902	1.826	2300	60	57	**54**	5,5	0,5
							51	1.448			2600	66	63	**61**		0,6
							90	1.826								
SM-S22-3	15	-108.13253	44.615	Madison	125-59E	N045	0	1.294	1.294	0.458	2450	61	**58**	53	7	0,38
							55	0.735			2800	67	**66**	61		0,17
							90	0.458								

[1]: orientation after correction from local bedding attitude; *Crossover length Lc given within 23% of uncertainty; **Range of depth consiedered based on burial model (see text for details)

Vertical principal stress is reported in bold, horizontal principal stresses are calculated considering for the Phosphoria (E=41 Gpa, v=0.25, μ=0.24 J/m²) and for the Madison (E=29 Gpa, v=0.2;μ=0.24 J/m²)

Table 1: Location of samples and results of inversion of tectonic stylolite roughness for stress in the Little Sheep Mountain – Sheep Mountain anticlines, USA.

Figure S1: Results of stylolite roughness inversion, per sample in the Little Sheep Mountain anticline. A- Crossover lengths L_c are reported as crosses within 23% uncertainty for the three cuts, B- Reconstructed periodic anisotropy for the corresponding samples, red squares are Lc, dotted line represents the vertical plane with respect to the orientation of the stylolite before strata tilting.

Figure S2: Results of stylolite roughness inversion, per sample in the Sheep Mountain anticline. Crossover lengths L_c are reported as crosses within 23% uncertainty for the three cuts, B- Reconstructed periodic anisotropy for the corresponding samples, red squares are L_c, dotted line represents the vertical plane with respect to orientation of the stylolite before strata tilting.

Figure S3: Results of stylolite roughness inversion, per sample in the Sheep Mountain anticline. Reconstructed periodic anisotropy for the corresponding samples presented on Figure S2, red squares are L_c, dotted line represents the vertical plane with respect to orientation of the stylolite before strata tilting.